Journal of Solid State Chemistry 183 (2010) 458–464

Contents lists available at ScienceDirect

Journal of Solid State Chemistry

journal homepage: www.elsevier.com/locate/jssc

# Crystal growth, crystal structure of new polymorphic modification, β-$Bi_2B_8O_{15}$ and thermal expansion of α-$Bi_2B_8O_{15}$

R.S. Bubnova [a], J.V. Alexandrova [b], S.V. Krivovichev [a,b], S.K. Filatov [b,*], A.V. Egorysheva [c]

[a] Grebenshchikov Institute of Silicate Chemistry, Russian Academy of Sciences, Makarov Emb 2, 199053 St.Petersburg, Russia
[b] Department of Crystallography, St. Petersburg State University, Universitetskaya nab. 7/9, 199034 St.Petersburg, Russia
[c] Kurnakov Institute of General and Inorganic Chemistry of the Russian Academy of Sciences, Leninsky Prospect 31, GSP-1, Moscow 119991, Russia

ARTICLE INFO

*Article history:*
Received 2 September 2009
Received in revised form
30 October 2009
Accepted 21 November 2009
Available online 2 December 2009

*Keywords:*
Bismuth borate
Crystal structure determination
Thermal expansion
Thermal phase transition

ABSTRACT

Single crystals of α- and β-polymorphs of $Bi_2B_8O_{15}$ were grown by Czochralski method from a charge of the stoichiometric composition. The crystal structure of β-$Bi_2B_8O_{15}$ was solved by direct methods from a twinned crystal and refined to $R1=0.081$ ($wR=0.198$) on the basis of 1584 unique observed reflections ($I>2\sigma(I)$). The compound is triclinic, space group $P\bar{1}$, $a=4.3159(8)$, $b=6.4604(12)$, $c=22.485(4)$ Å, $\alpha=87.094(15)^\circ$, $\beta=86.538(15)^\circ$, $\gamma=74.420(14)^\circ$, $V=602.40(19)$ Å$^3$, $Z=2$. The B–O layered anion of β-$Bi_2B_8O_{15}$ is topologically identical to the anion of α-$Bi_2B_8O_{15}$ but the orientation of neighboring layers is different. Thermal expansion of α-$Bi_2B_8O_{15}$ has been investigated by X-ray powder diffraction in air in temperature range from 20 to 700 °C. It is strongly anisotropic, which can be explained by the hinge mechanism applied to chains of Bi–O polyhedra. While the anisotropy of thermal expansion is rather high, the volume thermal expansion coefficient $\alpha_V=40\times10^6\,^\circ C^{-1}$ for α-$Bi_2B_8O_{15}$ is close to those of other bismuth borates.



## 1. Introduction

The growing interest to the bismuth borates is due to the discovery of nonlinear optical properties of $BiB_3O_6$ [1,2]. This fact made it possible to use it in nonlinear optics for producing solid-state ultraviolet lasers. Bismuth borates are luminophores with a high radiation resistance and can exhibit stimulated Raman scattering. Thus, they have a good potential for being used as laser radiation converters.

Stable phase equilibria in the $Bi_2O_3$–$B_2O_3$ were determined experimentally in [3] and the metastable equilibria were reported in [4]. Phase transition in $Bi_2B_8O_{15}$ was discovered in [3] and later confirmed in [5]. The temperature of phase transition is determined as 696 °C and the melting temperature is 715 °C. Crystal growth experiments of low-temperature α-$Bi_2B_8O_{15}$ polymorph from stoichiometric melt and by the Czochralski method were described in [6] and [7], respectively. First X-ray diffraction data for both modifications were reported in [3], and the unit cell parameters and symmetry were determined for α-$Bi_2B_8O_{15}$ in [6]. The crystal structure of low-temperature modification, α-$Bi_2B_8O_{15}$, was reported in [5,8]. The polymorph crystallizes in the monoclinic system, space group $P2_1$, $a=4.314$, $b=22.150$, $c=6.469$ Å, $\beta=105.49^\circ$, $Z=2$. Narrow region of homogenous solid solutions has been revealed based on α-$Bi_2B_8O_{15}$ [7] and crystal structure of the α-$Bi_2B_8O_{15}$ $(Bi_2O_3)_{0.06}$ solid solution was refined, although authors have not refined the position of the excess Bi atoms [7]. Although crystal structures for most of the homometallic compounds in the $Bi_2O_3$–$B_2O_3$ system have already been reported; the crystal structure of β-modification of $Bi_2B_8O_{15}$ has not been known. Its powder X-ray diffraction pattern, symmetry and unit cell parameters were previously reported [5] as following: triclinic, space group $P\bar{1}$, $a=6.055$, $b=7.704$, $c=8.016$ Å, $\alpha=100.90^\circ$, $\beta=105.43^\circ$, $\gamma=103.71^\circ$.

In this work, we describe the crystal growth of β- and α-$Bi_2B_8O_{15}$ by the Czochralski method, the results of structure determination for β-$Bi_2B_8O_{15}$, and thermal expansion of α-$Bi_2B_8O_{15}$.

## 2. Experimental

### 2.1. Crystal growth

Single crystals of the low- and the high-temperature phases $Bi_2B_8O_{15}$ were grown by the Czochralski method from a stoichiometric mixture of $Bi_2O_3$ (99.999%) and $H_3BO_3$ (99.999%). The melt had high viscosity and a tendency to glass formation and liquid–liquid phase separation [3,4], which determined the conditions for crystal growth. Crystals were grown in a resistance furnace in a platinum crucible 90 $cm^3$ volume. To ensure the homogeneity of

* Corresponding author.
*E-mail address:* filatov@crystalspb.com (S.K. Filatov).

0022-4596/$ - see front matter © 2009 Elsevier Inc. All rights reserved.
doi:10.1016/j.jssc.2009.11.021

the melt, the powdered compound previously obtained by solid-phase synthesis was loaded into the crucible. Supercooling temperature was the only growth condition that differed in the case of the low- and the high-temperature modifications. It was in the range 2–4 K for high-temperature phase and 20 K for low-temperature phase $Bi_2B_8O_{15}$ (i.e. at the temperature below the phase transition). The other conditions were the same for α- and β-modifications. Initially, polycrystalline tablets from pre-synthesized $Bi_2B_8Oi_5$ powder were made and one of the tablets was then used as a seed. The crystals were grown at the constant temperature. The pulling rate was 0–0.2 mm/h, the rotation velocity was 1.5–6 rpm. The axial temperature gradient above the melt was 0.8 K/cm. In both cases, bulky conglomerates of crystals were obtained and consisted of thin colorless plates $< 0.5$ mm thickness and with the maximal size up to 2 $cm^2$.

Powder samples of β-$Bi_2B_8O_{15}$ were prepared from mixed stoichimetric amounts of $Bi_2O_3$ (99.999%) and $H_3BO_3$ (99.9%). The mixture was pressed to form tablets, which were sintered at 680 °C for 3 h. The ceramic samples β-$Bi_2B_8O_{15}$ were heat treated at temperatures near to phase transition (below and above). The ratio of the polymorphic phases changes (depending on the treatment time and temperature); and at 710 °C β-$Bi_2B_8O_{15}$ completely transformed into the α-phase. On cooling, α-$Bi_2B_8O_{15}$ transformed into β-phase at 675 °C, evidencing that the phase transition is reversible and is of the first order.

### 2.2. Crystal-structure determination

The crystal chosen for data collection was examined with optical microscope and mounted on a glass fiber. Data were collected by means of a STOE IPDS II diffractometer using monochromated Mo$K\alpha$ radiation and frame widths of 2° in $\omega$. The unit-cell dimensions (Table 1) were refined by least-square techniques. The data were corrected for Lorentz, polarization, absorption, and background effects. The intensity statistics indicated the space group $P\bar{1}$. During the indexing, it has been found that the crystal studied was twinned along the (001) plane. Attempts to find untwinned crystal were unsuccessful and the structure was solved and refined by means of the programs SIR-92 [9] and SHELXL-97 [10], respectively. Unfortunately, it was not possible to separate contributions from different twin components into the diffraction pattern that resulted in quite high $R1$ index of 0.081. The solution in non-centrosymmetric group $P1$ did not provide essential improvement but led to severe correlations problems. The final models included anisotropic displacement parameters for cations only. Attempts to refine B and O anisotropically resulted in physically unrealistic displacement parameters that we tend to ascribe to the severe

**Table 1**
Crystal data for β-$Bi_2B_8O_{15}$.

| | |
|---|---|
| Crystal system | Triclinic |
| Space group | $P\bar{1}$ |
| $a$ (Å) | 4.3159(8) |
| $b$ (Å) | 6.4604(12) |
| $c$ (Å) | 22.485(4) |
| $\alpha$ (deg) | 87.094(15) |
| $\beta$ (deg) | 86.538(15) |
| $\gamma$ (deg) | 74.420(14) |
| $V$ (Å$^3$) | 602.40(19) |
| $Z$ | 2 |
| Range in $h$, $k$, $l$ | $-5 \le h \le 5$, $-8 \le k \le 8$, $-28 \le l \le 26$ |
| $\theta_{min} - \theta_{max}$ | 1.82 – 26.73 |
| Total number of reflections | 1803 |
| Reflections with $I > 2\sigma(I)$ | 1584 |
| $R_1$ | 0.0817 |
| $wR_2$ | 0.1985 |
| Goodness-of-fit | 1.199 |
| Min/max residual electron density | −2.518/3.184 |

**Table 2**
Atomic coordinates, equivalent isotropic thermal parameters $U_{eq}$ (Å$^2$) and bond valence sums (*BVS*, v.u.) for β-$Bi_2B_8O_{15}$.

| Atom | $x/a$ | $y/b$ | $z/c$ | $U_{eq}$ | *BVS* [14] | *BVS* [13] |
|---|---|---|---|---|---|---|
| Bi1 | 0.8733(3) | 0.38024(16) | 0.06739(6) | 0.0307(5) | 3.33 | 3.04 |
| Bi2 | 0.4117(3) | 0.89799(16) | 0.43200(6) | 0.0274(5) | 3.23 | 2.98 |
| O1 | 0.407(5) | 0.512(3) | 0.4364(10) | 0.023(4) | 1.97 | 1.98 |
| O2 | 0.884(6) | −0.010(4) | 0.0663(11) | 0.033(5) | 2.05 | 2.07 |
| O3 | 0.440(4) | 0.826(3) | 0.0703(8) | 0.015(4) | 2.23 | 2.27 |
| O4 | 1.354(6) | 0.217(4) | 0.0711(11) | 0.034(5) | 2.16 | 1.98 |
| O5 | −0.010(7) | 1.349(4) | 0.4378(12) | 0.042(6) | 1.84 | 1.88 |
| O6 | 0.907(5) | 0.733(3) | 0.4273(10) | 0.028(5) | 2.28 | 2.15 |
| O7 | 0.382(4) | 0.859(3) | 0.5265(9) | 0.016(4) | 2.20 | 1.99 |
| O8 | 0.877(5) | 0.372(3) | −0.0271(9) | 0.021(4) | 2.08 | 1.88 |
| O9 | 0.654(5) | 1.217(3) | 0.3715(10) | 0.027(5) | 2.35 | 2.39 |
| O10 | 0.919(6) | 0.328(4) | −0.1295(10) | 0.031(5) | 1.74 | 1.74 |
| O11 | 1.127(8) | 0.393(5) | −0.2208(14) | 0.058(8) | 2.15 | 2.15 |
| O12 | 1.097(9) | 0.040(5) | −0.1961(16) | 0.067(9) | 1.90 | 1.90 |
| O13 | 0.623(9) | 1.543(5) | 0.3176(15) | 0.067(9) | 1.75 | 1.75 |
| O14 | 0.591(10) | 1.894(6) | 0.2862(17) | 0.077(10) | 1.65 | 1.65 |
| O15 | 1.302(10) | −0.227(6) | −0.2681(17) | 0.076(10) | 2.60 | 2.60 |
| B1 | 0.349(7) | 0.690(4) | 0.5742(13) | 0.010(5) | 2.89 | 2.89 |
| B2 | 0.145(8) | 0.799(5) | 0.0729(16) | 0.022(7) | 3.19 | 3.19 |
| B3 | 0.072(8) | 1.529(5) | 0.4310(16) | 0.024(7) | 3.20 | 3.20 |
| B4 | 0.551(9) | 1.005(5) | 0.0671(17) | 0.025(7) | 2.82 | 2.82 |
| B5 | 0.662(11) | 1.313(7) | 0.320(2) | 0.038(9) | 3.27 | 3.27 |
| B6 | 1.030(12) | 0.247(7) | −0.183(2) | 0.043(10) | 3.18 | 3.18 |
| B7 | 1.253(17) | −0.037(11) | −0.253(3) | 0.072(17) | 3.02 | 3.02 |
| B8 | 0.697(16) | 1.671(10) | 0.270(3) | 0.062(14) | 2.97 | 2.97 |
| Atom | $U_{11}$ | $U_{22}$ | $U_{33}$ | $U_{23}$ | $U_{13}$ | $U_{12}$ |
| Bi1 | 0.0348(8) | 0.0133(6) | 0.0449(10) | −0.0028(5) | 0.0054(6) | −0.0091(5) |
| Bi2 | 0.0214(6) | 0.0145(6) | 0.0471(10) | −0.0008(4) | −0.0039(5) | −0.0059(4) |

**Table 3**
Main interatomic distances for β-$Bi_2B_8O_{15}$.

| Bond | *d* (Å) | Bond valence [14] | Bond valence [13] |
|---|---|---|---|
| Bi1–O4 | 2.06(2) | 1.07 | 0.86 |
| –O8 | 2.13(2) | 0.90 | 0.75 |
| –O8 | 2.28(2) | 0.60 | 0.54 |
| –O2 | 2.51(2) | 0.32 | 0.34 |
| –O4 | 2.72(2) | 0.18 | 0.22 |
| –O10 | 2.76(2) | 0.16 | 0.20 |
| –O3 | 2.98(2) | 0.09 | 0.13 |
| ⟨Bi(1)–O⟩$_3$/*BVS* | 2.16 | 2.57 | 2.15 |
| ⟨Bi(1)–O⟩$_7$/*BVS* | 2.49 | 3.33 | 3.04 |
| Bi2–O6 | 2.12(2) | 0.93 | 0.77 |
| –O7 | 2.13(2) | 0.90 | 0.75 |
| –O7 | 2.26(2) | 0.62 | 0.57 |
| –O1 | 2.50(2) | 0.33 | 0.35 |
| –O6 | 2.68(2) | 0.20 | 0.24 |
| –O9 | 2.81(2) | 0.14 | 0.18 |
| –O5 | 2.99(2) | 0.09 | 0.12 |
| ⟨Bi(2)–O⟩$_3$/*BVS* | 2.17 | 2.46 | 2.09 |
| ⟨Bi(2)–O⟩$_7$/*BVS* | 2.50 | 3.23 | 2.98 |
| B1–O9 | 1.38(4) | 0.96 | |
| –O1 | 1.46(3) | 0.79 | |
| –O7 | 1.52(3) | 0.67 | |
| –O5 | 1.59(4) | 0.55 | |
| ⟨B1–O⟩/*BVS* | 1.49 | 2.89 | |
| B2–O3 | 1.33(4) | 1.12 | |
| –O2 | 1.43(4) | 0.83 | |
| –O10 | 1.53(4) | 0.65 | |
| –O8 | 1.57(4) | 0.58 | |
| ⟨B2–O⟩/*BVS* | 1.47 | 3.19 | |
| B3–O5 | 1.30(4) | 1.20 | |
| –O6 | 1.32(4) | 1.15 | |
| –O1 | 1.43(4) | 0.85 | |
| ⟨B3–O⟩ | 1.35 | 3.20 | |
| B4–O3 | 1.36(4) | 1.02 | |
| –O4 | 1.41(4) | 0.90 | |
| –O2 | 1.41(4) | 0.89 | |
| ⟨B4–O⟩/*BVS* | 1.39 | 2.82 | |
| B5–O9 | 1.30(5) | 1.25 | |
| –O15 | 1.29(5) | 1.21 | |
| –O13 | 1.44(5) | 0.81 | |
| ⟨B5–O⟩/*BVS* | 1.35 | 3.27 | |
| B6–O12 | 1.34(5) | 1.11 | |
| –O10 | 1.35(5) | 1.07 | |
| –O11 | 1.37(5) | 1.01 | |
| ⟨B6–O⟩/*BVS* | 1.35 | 3.18 | |
| B7–O15 | 1.25(7) | 1.39 | |
| –O14 | 1.45(7) | 0.83 | |
| –O12 | 1.45(7) | 0.80 | |
| ⟨B7–O⟩/*BVS* | 1.38 | 3.02 | |
| B8–O11 | 1.32(6) | 1.14 | |
| –O13 | 1.39(7) | 0.94 | |
| –O14 | 1.44(7) | 0.81 | |
| ⟨B8–O⟩/*BVS* | 1.39 | 2.97 | |

effects of twinning. The final atomic positional and displacement parameters are given in Table 2. Selected interatomic distances are given in Table 3.

### 2.3. High-temperature X-ray powder diffraction study

Thermal expansion of α-$Bi_2B_8O_{15}$ was studied by high-temperature X-ray powder diffraction, using DRON-3 diffractometer, equipped with a high-temperature KRV-1100 chamber (Cu*K*α-radiation, 35 kV, 20 mA). Thermal expansion was investigated in the temperature range of 20–420 °C with 30 °C step and in the range of 420–700 °C with 40 °C step. $2\theta$ range is 6–60°. The unit cell parameters for all temperatures studied were calculated using the least-square method, whereas the $\alpha$ and $\beta$ parameters increase on heating almost linearly, temperature dependencies of the *b* and *c* parameters show a kink at ~300 °C (see Fig. 4). As the temperature dependence of *b* and *c* has special points, those dependencies were approximated linearly within 20–300 and 300–660 °C intervals. 20–300 °C: $a=4.320+0.00000765\times t$, $b=22.166+0.00109713\times t$, $c=6.491-0.00004799\times t$, $\beta=105.56+0.00006533\times t$; 300–660 °C: $\alpha=4.320+0.00000765\times t$, $b=22.286+0.00067412\times t$, $c=6.459+0.00005453\times t$, $\beta=105.56+0.00006533\times t$. Main coefficients of the thermal expansion tensor including its orientation with respect to crystallographic axes were determined using linear approximation of temperature dependencies for the unit-cell parameters by Belousov and Filatov program [11].

## 3. Results and discussion

### 3.1. The crystal structure

#### 3.1.1. Cation and anion coordination

There are two symmetrically non-equivalent Bi atoms in β-$Bi_2B_8O_{15}$ coordinated by seven O atoms each (Fig. 1b). Variations of bond lengths in both $BiO_7$ polyhedra are 2.06–2.99 Å, and the average bond length is 2.49 Å (Table 3). For the sake of simplicity, it is convenient to describe the Bi coordination polyhedra as consisting of the oxygen atoms that have strong Bi–O interactions only and the lone electron pair [12,13], etc. Three short bonds in the $Bi(1)O_7$ polyhedron (black color in Fig. 1a and b) are in the range of 2.06–2.28 Å, and other ligands are located at 2.51–2.98 Å. If we choose three short bonds for the $Bi^{3+}$ coordination, the coordination polyhedron is $Bi(1)O_3$ trigonal pyramid with $Bi^{3+}$ in its apex. In a similar manner, a trigonal $Bi(2)O_3$ pyramid can be considered (Fig. 1a and b). The bond-length-intervals for the $BiO_3$ polyhedra are 2.06–2.28 Å and the average bond length is 2.16 Å.

There are eight symmetrically independent B atoms in β-$Bi_2B_8O_{15}$ structure (Fig. 2). B(3), B(4), B(5), B(6), B(7) and B(8) atoms are coordinated by three O atoms each. The B–O bond lengths in the $BO_3$ triangles vary from 1.25 to 1.45 Å, with the average bond length of 1.37 Å (Table 3). B(1) and B(2) atoms are tetrahedrally coordinated by four O atoms each. The B–O bonds in $BO_4$ tetrahedra are in the range of 1.33–1.59 Å, and the average bond length is 1.48 Å. The O–B–O angles vary from 109° to 134° for the $BO_3$ triangles and from 97° to 117° for the $BO_4$ tetrahedra.

The O(11), O(12), O(13), O(14) and O(15) atoms are coordinated by two B atoms, i.e. they are bridging ligands in the borate anion (see below). The O(1), O(2), O(3), O(5), O(4), O(6), O(7), O(8), O(9) and O(10) atoms are terminal and bonded to one or two Bi atoms as well.

Bond-valence sums (*BVS*) for atoms in the β-$Bi_2B_8O_{15}$ structure are listed in Tables 2 and 3. They have been calculated using the bond–valence parameters for all the bonds from [14], and in addition from [13] for the Bi–O bonds ($r_0$=1.990 Å, *b*=0.48).

#### 3.1.2. Structure of the borate anion

The borate anion can be described as consisting of six borate basic units: the triborate group of three triangles (B(6), B(7) and B(8) atoms), two single $BO_4$ tetrahedra (B(1) and B(2)) and three single $BO_3$ triangle (formed by B(3), B(4) and B(5) atoms) (Fig. 2). According to the modern descriptions of borate groups by Touboul et al. [15] and Burns et al. [16], the asymmetric unit is symbolized as $8:\infty^2[(1:\Delta)+(1:T)+(3:3\Delta)+(1:\Delta)+(1:T)+(1:\Delta)]$ or 8B: $\Delta\square\langle 3\square\rangle\Delta\square\Delta$, respectively, where 8B means eight boron atoms composing the asymmetric unit and the $BO_4$ tetrahedron

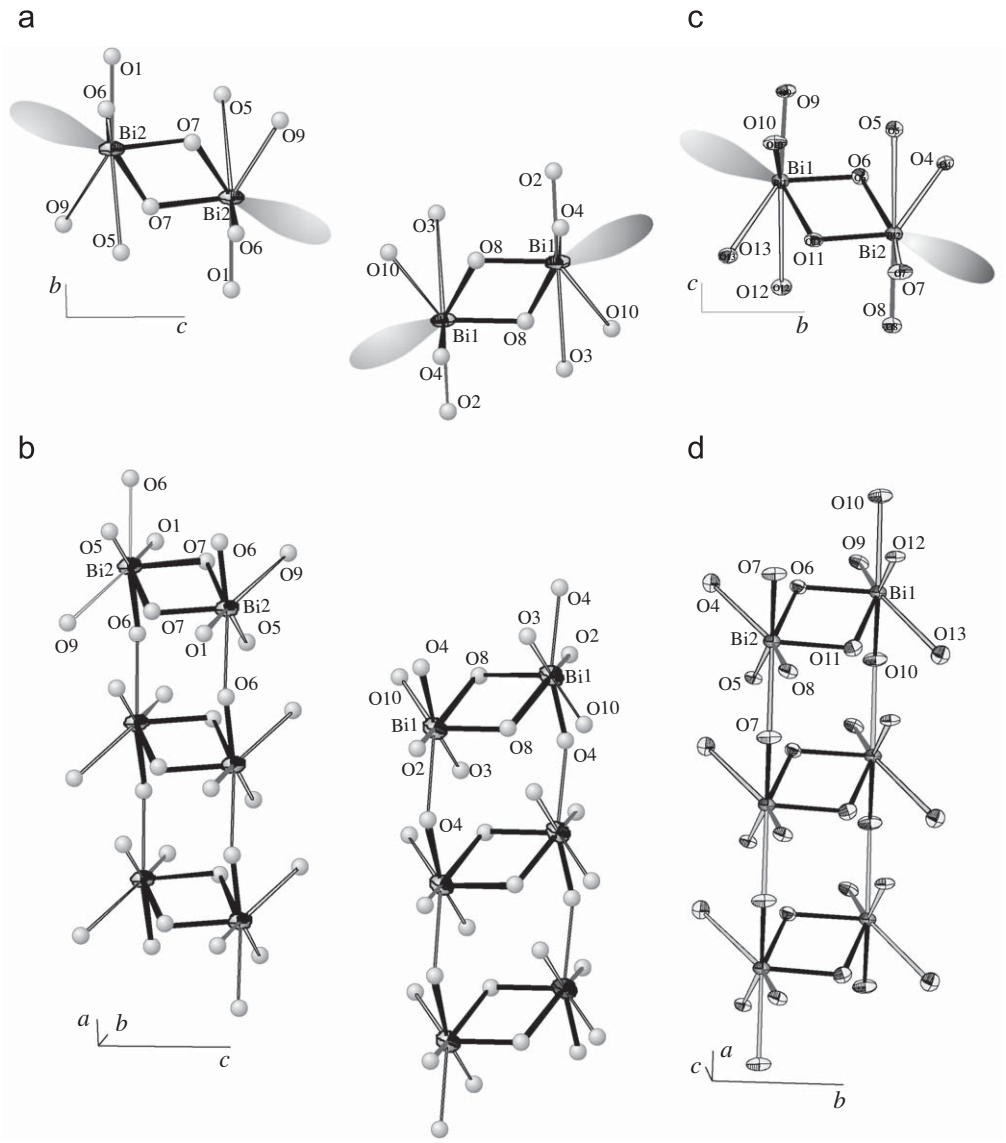


**Fig. 1.** Comparison of bismuthate groups and chains of β-$Bi_2B_8O_{15}$ (a–b) and α-$Bi_2B_8O_{15}$ (c–d) crystal structures.

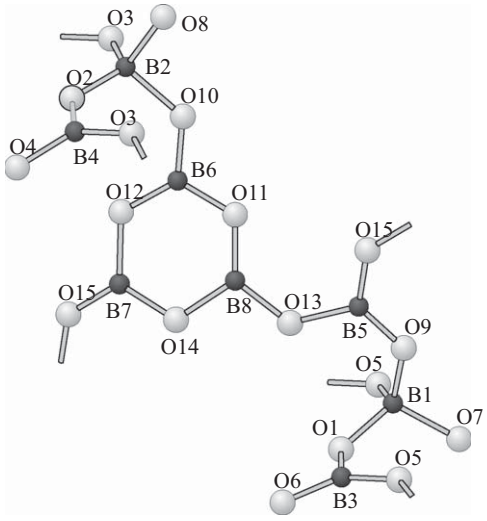


**Fig. 2.** Independent part of borate anion of β-$Bi_2B_8O_{15}$.

stands for T or □, respectively, whereas the $BO_3$ triangle stands as Δ. The notation $\infty^2$ in Touboul's notation means 2D-dimensionality of the borate anion. The symbol of the triborate group is 3:3 T [15] or 3B:⟨3⟩ [16], in the last notation the < > delimiters indicate that borate polyhedra form a ring.

The triborate rings and B(5)$O_3$ triangles linked with each other by apices to form chains along the *b* axis (Fig. 2 and 3a). The B(1)$O_4$ tetrahedra are linked to B(3)$O_3$ triangles by apices to form chains running along the *a* axis. In a similar manner, the B(2)$O_4$ tetrahedra and B(4)$O_3$ triangles form chains running along the *a* axis (Fig. 3b). These chains connect to each other forming triple open layers, parallel to the *ab* plane. The central part of the layer is formed by chains of triborate rings and $BO_3$ triangles, whereas chains of $BO_4$ tetrahedra and $BO_3$ triangles are located on the sides of the layer.

### 3.1.3. Bismuthate groups

Two distorted Bi(1)$O_7$ polyhedra share a common edge O(8)–O(8) to form $[Bi(1)_2O_{10}]^{14-}$ groups, by analogy, two Bi(2)$O_7$

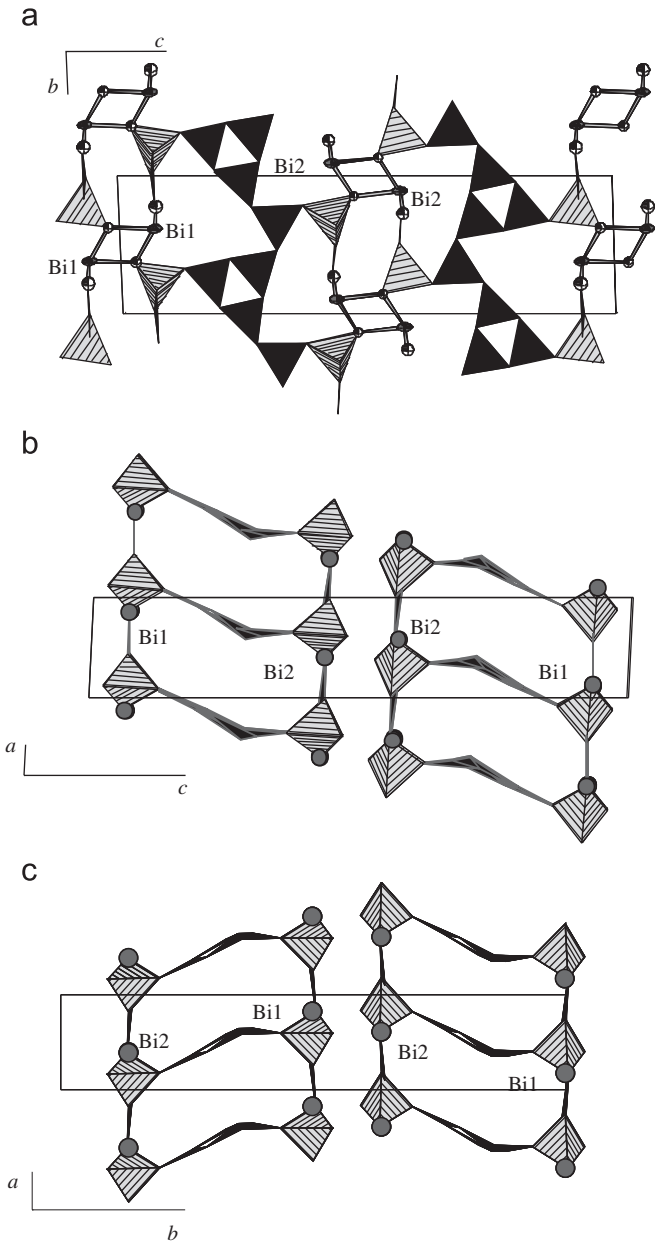


**Fig. 3.** Comparison of crystal structures of β-$Bi_2B_8O_{15}$ projected onto *bc* (a), *ac* (b) planes and α-$Bi_2B_8O_{15}$ (c).

polyhedra linked with each other by a common edge O(7)–O(7) to form similar $[Bi(2)_2O_{10}]^{14-}$ groups (Fig. 1a). The Bi(1)–Bi(1) and Bi(2)–Bi(2) bond lengths are close to each other and equal to 3.579 and 3.592 Å, respectively. These double groups sharing a common edge are typical for the Bi-containing compounds and have been observed in α-$Bi_2B_8O_{15}$ [5,7,8], $Bi_3B_5O_{12}$ [17], $BaBi_2B_4O_{10}$ [18], etc. For the abridged BiO-polyhedra (see above) the $Bi_2O_4$ groups can be considered consisting of the $BiO_3$ distorted trigonal pyramids (shown black in Fig. 1a and b). Two Bi(1) atoms and two O(8) atoms in the group form a rhomb in the *bc* plane. Similar rhombs are formed by two Bi(2) atoms and two O(7) atoms (Fig. 1a). These rhombs can be considered as the most rigid units of the structure, as it was proposed in [18]. The $[Bi(1)_2O_{10}]^{14-}$ groups are connected via two common O(4) atoms and the $[Bi(2)_2O_{10}]^{14-}$ groups are connected via two common O(6) atoms to form two independent bismuthate chains running along the *a* axis (Fig. 1b).

### 3.1.4. Structure description

The structure of β-$Bi_2B_8O_{15}$ is shown in Fig. 3a and b. The borate layers sharing common bismuthate chains extend along *a* axis to form a framework. The bismuthate chains are in between the chains of $BO_4$ tetrahedra and $BO_3$ triangles. Six Bi–O bonds from the $BiO_7$ polyhedra are located in the plane of the layer and the remaining bond (either Bi(1)–O(8) or Bi(2)–O(7)) connect layers to each other. As a result, the layers are linked via the Bi–O rhombs (Fig. 3b).

The same borate layers occur in the structure of α-$Bi_2B_8O_{15}$. Different symmetry of α- (monoclinic, $P2_1$) and β- (triclinic, $P\bar{1}$) phases of $Bi_2B_8O_5$ is due to the different orientation of borate layers in these phases (Fig. 3b and c). The *b* axis in the α-$Bi_2B_8O_{15}$ phase corresponds to the *c* axis in the β-$Bi_2B_8O_{15}$ phase. The borate layers in the structure of α-$Bi_2B_8O_{15}$ are related by the $2_1$ screw axis, since they are rotated by 180° with respect to each other and shifted by a half of the *b* translation. In contrast, in β-$Bi_2B_8O_{15}$, adjacent borate layers are related by the inversion center $\bar{1}$. Since β- and α-phases of $Bi_2B_8O_{15}$ are different by the layer stacking only, they can be considered as polytypes. It is of interest that the bismuthate chains formed by the $[Bi_2O_{10}]^{14-}$ groups exist in α-$Bi_2B_8O_{15}$ as well (Fig. 1d). Variation of the Bi–O bond lengths in α-$Bi_2B_8O_{15}$ is 2.06–2.89 Å, and the average bond length is 2.42 Å. The $Bi(1)O_7$ and $Bi(2)O_7$ polyhedra share a common edge O6–O11 to form $[Bi_2O_{10}]^{14-}$ groups (Fig. 1c), and the Bi(1)–Bi(2) distance is equal to 3.576 Å. Thus only one type of bismuthate chains exists in α-$Bi_2B_8O_{15}$ in contrast to two independent bismuthate chains in β-$Bi_2B_8O_{15}$.

## 3.2. Thermal expansion of α-$Bi_2B_8O_{15}$ crystal structure

Thermal expansion of α-$Bi_2B_8O_{15}$ has a strongly anisotropic character: the structure expands intensively along *b* axis and shows almost no expansion in the perpendicular plane.

The character of temperature dependencies of *b* and *c* parameters changes at about 300 °C (Fig. 4): in the temperature range of 20–300 °C, $\alpha_{11}=2$, $\alpha_{22}=\alpha_b=49$, $\alpha_{33}=-8$, $\alpha_V=43$, $\langle\alpha\rangle=\alpha/3=14\times10^{-6}\,°C^{-1}$, $\mu=11°$ (counterclockwise), $\alpha_a=2$, $\alpha_c=-7\times10^{-6}\,°C^{-1}$; in temperature range of 300–700 °C $\alpha_{11}=8$, $\alpha_{22}=\alpha_b=30$, $\alpha_{33}=2$, $\alpha_V=40$, $\langle\alpha\rangle=13\times10^{-6}\,°C^{-1}$, $\mu=87°$ (clockwise), $\alpha_a=2$, $\alpha_c=8\times10^{-6}\,°C^{-1}$. The thermal expansion coefficient figures in comparison to crystal structures are shown in Fig. 5.

The puckered pseudo-layers running along *b* axis are linked by truncated $Bi_2O_4$ groups to form framework in α-$Bi_2B_8O_{15}$ (Fig. 5b). The hinge mechanism may be used to explain this simultaneous change of lattice constants. The extension of three-dimensional hinge along certain direction (the *b* axis) should be obviously accompanied by simultaneous contraction of the structure in the perpendicular direction (the *a* axis). The common thermal expansion of the structure superimposes on the contraction, and the structure has almost no expansion along the *a* axis.

It is very probable that the Bi–O rhomb is a cell of the hinge in this structure. The maximal axes of the $Bi^{3+}$ displacement ellipsoids are oriented along the *b* axis (Fig. 5b). The Bi(1)–Bi(2) distance in the $Bi_2O_2$ rhomb is 3.576 Å, which is certainly larger than the sum of the $Bi^{3+}$ ionic radii (3.20 Å). At lower temperatures, two Bi atoms do not interact with each other and the structure expands strongly along maximal ellipsoids axes and contracts along the other directions of the hinge. At higher temperatures, the atomic repulsion causes changes in the character of thermal expansion change. That mechanism of thermal expansion was considered in detail in [19] where it was termed a "switching" of the hinge mechanism. In particular this mechanism is realized in the thermal expansion of $BaBi_2B_4O_{10}$ [18,19].

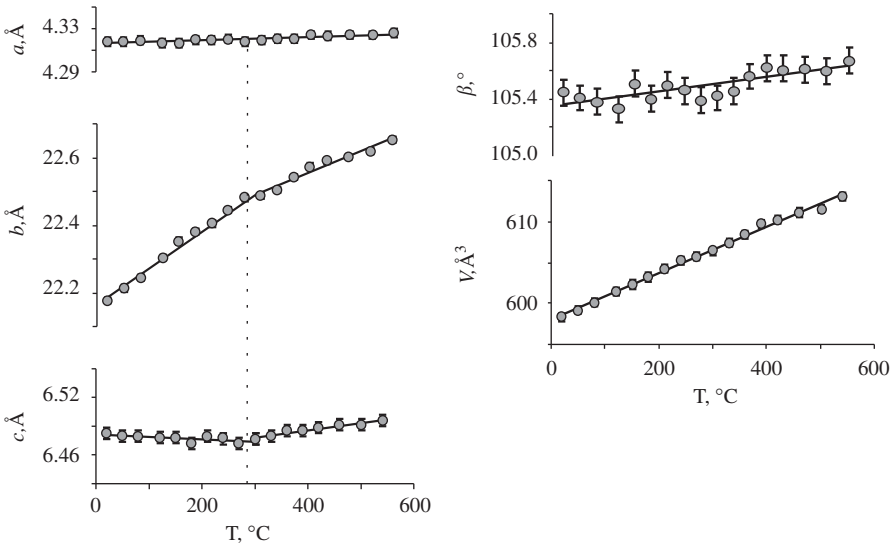


**Fig. 4.** The temperature dependencies of parameters unit cell of α-$Bi_2B_8O_{15}$.

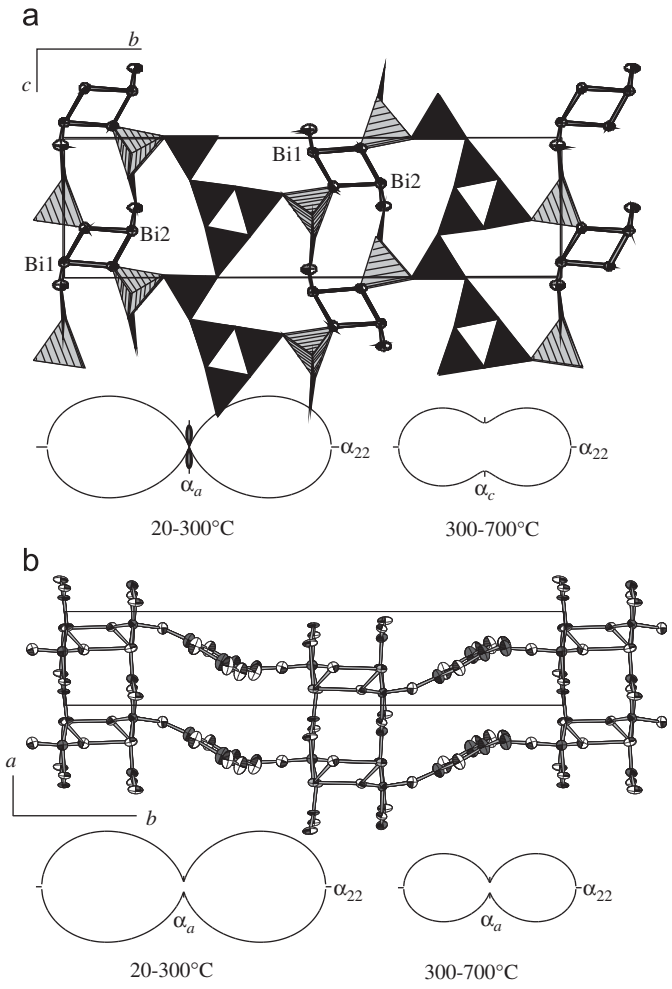


**Fig. 5.** Correlation between the coefficients of thermal expansion tensor and the structure of α-$Bi_2B_8O_{15}$ projected onto *bc* (a) and *ab* (b) planes.

The value of the coefficient of volume thermal expansion $\alpha_V$=42 × $10^{-6}$ °$C^{-1}$ for α-$Bi_2B_8O_{15}$ is less than average that over univalent borates (65 × $10^{-6}$ °$C^{-1}$) [20–22], whereas it is close to those over divalent (42 × $10^{-6}$ °$C^{-1}$) [21] and other bismuth borates, 41 × $10^{-6}$ °$C^{-1}$ for $Bi_4B_2O_9$ [23], 27 × $10^{-6}$ °$C^{-1}$ for $Bi_3B_5O_{12}$ [17], (34–39) × $10^{-6}$ °$C^{-1}$ for $BiB_3O_6$ [24,25], 40 × $10^{-6}$ °$C^{-1}$ for $BaBi_2B_4O_{10}$ [18] and 24 × $10^{-6}$ °$C^{-1}$ for $SrBi_2B_4O_{10}$ [26] as well as it is close to average over Bi-borates (38 × $10^{-6}$ °$C^{-1}$) [21,22]. Decreasing of thermal expansion of Bi-borates is caused by increasing of strength of metal–oxygen chemical bond [21,22].

## 4. Conclusions

The $\alpha \leftrightarrow \beta$ polymorph transition under study is the first-order phase transition. The crystal structure of the β-modification of $Bi_2B_8O_{15}$ demonstrated that the B–O layered anion is topologically identical to the anion in α-$Bi_2B_8O_{15}$ modification. The difference between the α- and β-phases is due to the different stacking sequences of borate layers in these structures, therefore they can be considered as polytypes.

The α-$Bi_2B_8O_{15}$ phase demonstrates very complicated thermal expansion. Temperature dependences for *b* and *c* monoclinic unit cell parameters exhibit pronounced kinks at about 300 °C. Highly anisotropic thermal oscillations of the Bi atoms and rigid Bi–O bonds result in highly anisotropic thermal expansion that can be described as switching of hinge mechanism of the Bi–O polyhedra. This process complicates a general thermal expansion of crystals. The intensity of atomic vibrations in a direction of the longest vibration amplitudes can be sharply increased. In this case on heating above a certain temperature (300 °C), neighboring cations start to repel each other along this direction—an additional mechanism of thermal deformations switches on. The phenomenon demonstrates itself as special points on temperature dependence for unit cell parameters. In spite of high anisotropy of thermal expansion the value of the coefficient of volume thermal expansion for α-$Bi_2B_8O_{15}$ is close to those of other bismuth borates.

## Acknowledgments

This research has been supported by the Russian Foundation for Basic Research through Grants no. 08-03-00232 for R.S.B, J.V.A., S.V.K and S.K.F., and Federal Agency on Science and Innovations (state Contract 02.740.11.0326).

## Appendix A. Supplementary material

Supplementary data associated with this article can be found in the online version at doi:10.1016/j.jssc.2009.11.021.

## References

[1] H. Hellwig, J. Liebertz, L. Bohatý, Solid State Commun. 109 (1999) 249–251.
[2] H. Hellwig, J. Liebertz, L. Bohatý, J. Appl. Phys. 88 (2000) 240–244.
[3] E.M. Levin, C.L. McDaniel, J. Am. Ceram. Soc. 45 (1962) 355–360.
[4] Yu.F. Kargin, V.P. Zhereb, A.V. Egorysheva, Russ. J. Inorg. Chem. 47 (2002) 1240–1242 (Translated from Zh. Neorg. Khim. 47 (2002) 1362–1364).
[5] A.V. Egorysheva, A.S. Kanishcheva, Yu.F. Kargin, Yu.E. Gorbunova, Yu.N. Mikhailov, Russ. J. Inorg. Chem. 47 (2002) 1804–1808 (Translated from Zh. Neorg. Khim. 47 (2002) 1961–1965).
[6] P. Becker, P. Held, Cryst. Res. Technol. 36 (2001) 1353–1356.
[7] F.Yu. Zavartsev, G.M. Kuz'micheva, V.B. Rybakov, S.A. Kutovoï, A.I. Zagumennyï, Crystallogr. Rep. 51 (2006) 705–709 (Translated from Kristallogr. 51 (2006) 748–753).
[8] B. Teng, W.T. Yu, J.Y. Wang, X.F. Cheng, S.M. Dong, Y.G. Liu, Acta Crystallogr. C 58 (2002) i25–i26.
[9] A. Altomare, G. Cascarano, C. Giacovazzo, A. Guagliardi, M.C. Burla, G. Polidori, M. Camalli, J. Appl. Crystallogr. 27 (1994) 435.
[10] G.M. Sheldrick, SHELXL-97, Program for the Refinement of Crystal Structures, Universität Göttingen, Germany, 1997.
[11] R.I. Belousov, S.K. Filatov, Glass Phys. Chem. 33 (2007) 271–275.
[12] S.V. Krivovichev, S.K. Filatov, Acta Crystallogr. B 55 (1999) 664–676.
[13] S.V. Krivovichev, S.K. Filatov, Crystal Chemistry of Minerals and Inorganic Compounds with Complexes of Anion Centered Tetrahedra, St.Petersburg State University, 2001 (in Russ.).
[14] N.E. Brese, M. O'Keeffe, Acta Crystallogr. B 47 (1991) 192–199.
[15] M. Touboul, N. Penin, G. Nowogrocki, Solid State Sci. 5 (2003) 1327–1342.
[16] P.C. Burns, J.D. Grice, F.C. Hawthorne, Can. Miner. 22 (1995) 1131–1151.
[17] S.K. Filatov, Ju.F. Shepelev, R.S. Bubnova, N.A. Sennova, A.V. Egorysheva, Yu.F. Kargin, J. Solid State Chem. 177 (2004) 515–522.
[18] R.S. Bubnova, S.V. Krivovichev, S.K. Filatov, A.V. Egorysheva, Y.F. Kargin, J. Solid State Chem. 180 (2007) 596–603.
[19] S.K. Filatov, R.S. Bubnova, Z. Kristallogr. S 26 (2007) 447–452.
[20] S.K. Filatov, R.S. Bubnova, Phys. Chem. Glasses 41 (2000) 216–224.
[21] R.S. Bubnova, S.K. Filatov, Phys. Stat. Sol. 245 (2008) 2469–2476.
[22] R.S. Bubnova, S.K. Filatov, High Temperature Crystal Chemistry of Borates and Borosilicates, St. Petersburg, Nauka, 2008 (in Russ.).
[23] S.K. Filatov, Y.F. Shepelev, J.V. Aleksandrova, R.S. Bubnova, Russ. J. Inorg. Chem. 52 (2007) 21–28 (Translated from Zh. Neorg. Khim. 52 (2007) 26–33).
[24] P. Becker, L. Bohatý, Cryst. Res. Technol. 36 (2001) 1175–1180.
[25] W.-D. Stein, A. Cousson, P. Becker, L. Bohatý, M.Z. Braden, Kristallogr. 222 (2007) 680–689.
[26] M.G. Krzhizhanovskaya, R.S. Bubnova, A.V. Egorysheva, M.S. Kozin, V.D. Volodin, S.K. Filatov, J. Solid State Chem. 182 (2009) 1260–1264.